Model Reference Adaptive Controller for Simultaneous Voltage and Frequency Restoration of Autonomous AC Microgrids

Farahnaz Ahmadi, Yazdan Batmani, and Hassan Bevrani, *IEEE*, *Fellow*

***Abstract*—In an autonomous droop-based microgrid, the system voltage and frequency (VaF) are subject to deviations as load changes. Despite the existence of various control methods aimed at correcting system frequency deviations at the secondary control level without any communication network, the challenges associated with these methods and their abilities to simultaneously restore microgrid VaF have not been fully investigated. In this paper, a multi-input multi-output (MIMO) model reference adaptive controller (MRAC) is proposed to achieve VaF restoration while accurate power sharing among distributed generators (DGs) is maintained. The proposed MRAC, without any communication network, is designed based on two methods: droop-based and inertia-based methods. For the microgrid, the suggested design procedure is started by defining a model reference in which the control objectives, such as the desired settling time, the maximum tolerable overshoot, and steady-state error, are considered. Then, a feedback-feedforward controller is established, of which the gains are adaptively tuned by some rules derived from the Lyapunov stability theory. Through some simulations in MATLAB/SimPowerSystem Toolbox, the proposed MRAC demonstrates satisfactory performance.**

***Index Terms*—AC microgid, communication-free secondary control, droop-based method, inertia-based method, model reference adaptive controller (MRAC), simultaneous voltage and frequency restoration.**

I. Introduction

DUE to concerns over global warming, rising electrical energy consumption, and the depletion of fossil fuels, renewable energy sources (RESs) have received significant attention. Microgrid, a relatively new concept, offers a means to integrate RESs into existing distribution networks. Microgrids are small power networks that can operate in either islanded or grid-connected mode [1]. In the islanded mode, it is crucial to maintain system voltage and frequency (VaF) close to their nominal values to ensure a continuous power supply to local loads. To achieve a safe and efficient operation, the active and reactive power including load power should be shared precisely among distributed generators (DGs) based on their power ratings. The control of an islanded microgrid is a challenging and complex task, as multiple control objectives must be achieved simultaneously.

To enhance the intelligence and flexibility of microgrids, a hierarchical control structure comprising three levels, i.e., primary control, secondary control, and tertiary control, has been extensively employed in microgrid control [2]-[4]. The primary control level is responsible for ensuring VaF stability and providing control over active and reactive power sharing among DGs [5]. The secondary control level is designed to address the VaF deviations introduced by the primary control level [6], [7]. The tertiary control level manages power flow between the microgrid and the main grid and facilitates economically optimal operation [8], [9]. The main objective of this paper is to address the simultaneous VaF restoration, which is included in the secondary control level.

The primary control usually consists of a droop controller, inner voltage and current control loops, and a virtual impedance [3], [7]. In order to improve power quality and power sharing, a virtual impedance method is proposed [10]-[12], where the output impedance is characterized as resistive, inductive, or complex impedance. Inner voltage and current control loops along with the droop controller are responsible for VaF stability and power sharing, respectively. The active power-frequency (P-ω) and reactive power-voltage amplitude (Q-E) droop control method has been identified as superior in primary control due to its high flexibility, reliability, and power sharing capability without relying on communication links among DGs [13]. However, the conventional droop control method is afflicted by a significant issue relating to VaF deviations, which are caused by the inherent trade-off between power sharing accuracy and the rate of voltage regulation. To mitigate VaF deviations resulting from droop control, secondary control methods are proposed [14], [15], which are typically classified into centralized, distributed, and decentralized ones. Detailed information about the secondary control methods is provided in [16]-[18].

To achieve secondary frequency control (SFC) only using local variables of DGs and eliminate the need for communication links among DGs, decentralized methods have been proposed. These SFC methods can be categorized as either proportional-regulator-based or proportional-integral-regulator-based methods depending on the type of controller used,

Manuscript received: May 2, 2023; revised: August 25, 2023; accepted: January 5, 2024. Date of CrossCheck: January 5, 2024. Date of online publication: February 5, 2024.

F. Ahmadi, Y. Batmani (corresponding author), and H. Bevrani are with Department of Electrical Engineering, University of Kurdistan, Sanandaj, Iran (e-mail: farahnaz.ahmadi@uok.ac.ir; y.batmani@uok.ac.ir; h.bevrani@uok.ac.ir).

DOI: 10.35833/MPCE.2023.000277

which are defined as P-SFC and PI-SFC methods, respectively. In [19] and [20], the P-SFC methods produce the same compensation value, thereby preserving the active power sharing attained by the primary controller. Nevertheless, the employed methods cannot completely restore the frequency to its desired value. To cope with this problem, the PI-SFC methods are suggested for the frequency restoration without any communication links. A practical PI-SFC method for the virtual synchronous generator (VSG) [21] and the decentralized optimal secondary controller [22], in which the parameters of PI controller are selected by finding the solution of a Riccati equation, is proposed to regulate the frequency. Nonetheless, these methods are ineffective if the DGs have different parameters or start-up conditions. Since there is no communication among the DGs, they follow their own local references, which leads to conflicts among DGs. Each DG endeavors to regulate the system frequency based on its settings, causing the power sharing to gradually deteriorate.

In [23], a small AC-signal injection technique is proposed to improve the accuracy of active power sharing among DGs and restore the frequency of the system. Although this technique addresses the issue of imprecise power sharing by injecting an additional AC signal into the output voltage of the DG and reconstructing the droop control, it is achieved by sacrificing the accuracy of the voltage performance. A switched secondary controller that combines the advantages of P-SFC and PI-SFC methods is proposed in [24]. This controller involves adopting P-SFC and PI-SFC methods in a predefined time protocol to achieve frequency restoration and real power sharing simultaneously without relying on communication links. However, the effectiveness of this controller is heavily reliant on the accuracy of the event detection strategy. Hence, any failure in the event detection mechanism can lead to deteriorated system performance.

Model reference adaptive systems (MRASs) are used to design adaptive controllers for different classes of uncertain dynamic systems. The fundamental concept is to adjust the controller parameters in such a way that the system output tracks a reference model output, acting as the desired trajectory [25]. Due to the existence of various types of uncertainties and unknown/unmodelled dynamics, the MRASs can be systematically applied in autonomous AC microgrids. The main challenge considered in this paper is to achieve simultaneous VaF restoration of AC microgrids while ensuring accurate power sharing among DGs without any communication links based on local measurement. To this end, an multi-input multi-output (MIMO) model reference adaptive controller (MRAC) is proposed, which can be based on two methods: droop-based and inertia-based methods. Furthermore, the proposed MRAC is independent of the parameters of the feeder line or the output impedance of DG. Consequently, it guarantees accurate power sharing among DGs. The significant contributions and key features of the proposed MRAC are as follows.

1) The proposed MRAC can be flexibly applied to two different AC microgrid types, i. e., droop-based and inertia-based microgrids.

2) Since the parameters of the controller are directly adjusted, there is no need to estimate the parameters of the system model. Therefore, this leads to a reduction in the computational burden.

3) The selected reference model has a fully decoupled structure, which enables the independent control of active and reactive power through two entirely separate control loops even in the presence of uncertainties.

4) The proposed MRAC offers the potential to attain appropriate power sharing with high droop coefficients in a droop-based AC microgrid without causing instability.

The rest of this paper is as follows. Section II describes the small-signal modeling of DGs. Section III describes the design procedure of the proposed MRAC. In Section IV, simulation results of the proposed MRAC in an autonomous AC microgrid are evaluated. The conclusion of this paper is presented in Section V.

II. Small-signal Modeling of DGs

The diagram of a DG equipped with the proposed MRAC is shown in Fig. 1, where each DG consists of three-phase voltage source inverters (VSIs) connected through an LC filter. The DG is connected to the point of common coupling (PCC) via a feeder line and supplies power to a local load. PWM is short for pulse width modulation. Figure 1 presents a detailed control schematic of the DG using a communication-free MIMO adaptive controller. The proposed MRAC generates compensation signals, indicated by u_1 and u_2, which are added to the measured active and reactive power to simultaneously restore the VaF of DG. Additionally, the accurate power sharing is guaranteed by implementing droop control and virtual impedance.

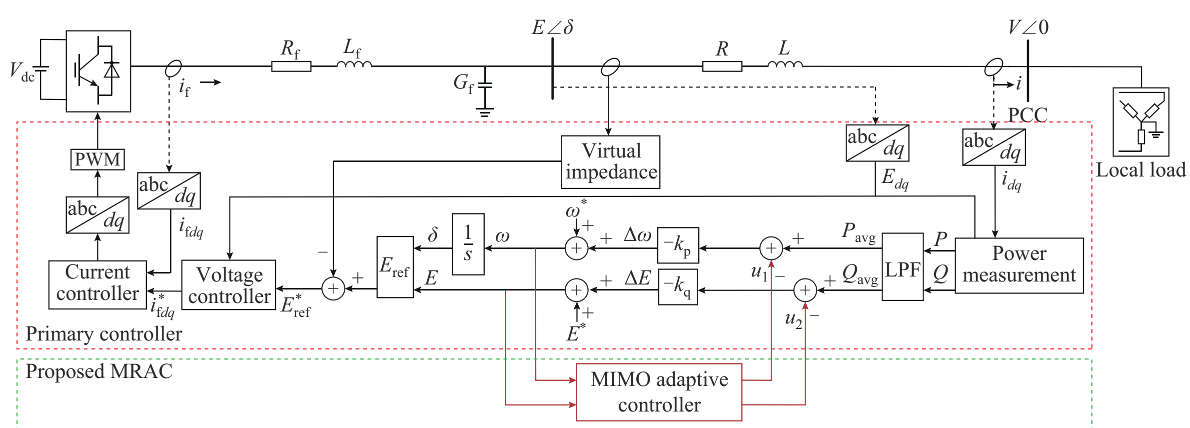

Fig. 1. Diagram of DG equipped with proposed MRAC.

A. Droop Control

The output active power P and reactive power Q of inverter can be formulated as [26]:

$$P=\frac{3}{R^2+X^2}(RE^2-REV\cos\delta+XEV\sin\delta) \tag{1}$$

$$Q=\frac{3}{R^2+X^2}(XE^2-XEV\cos\delta-REV\sin\delta) \tag{2}$$

where V and E are the amplitudes of the AC bus voltage and the inverter output voltage, respectively; R and X are the resistive and inductive components of the feeder line, respectively; and δ is the power angle.

If the line impedance is highly inductive ($R\approx 0$), the output active and reactive power of inverter can be reformulated as:

$$P=\frac{EV}{X}\sin\delta \tag{3}$$

$$Q=\frac{E(E-V\cos\delta)}{X} \tag{4}$$

Since δ is relatively small, $\sin\delta\approx\delta$ and $\cos\delta\approx 1$. Thus, the well-known droop-based method (P-ω and Q-E) can be rewritten as:

$$\omega=\omega^*-k_{\mathrm{p}}(P-P^*) \tag{5}$$

$$E=E^*-k_{\mathrm{q}}(Q-Q^*) \tag{6}$$

where k_{p} and k_{q} are the droop coefficients of frequency and voltage, respectively; P^* and Q^* are the active and reactive power references, respectively; and ω^* and E^* are the frequency and voltage references, respectively.

By assuming small disturbances around the equilibrium point defined as (δ_{e}, E_{e}, V_{e}), (1), (2), (5), and (6) can be linearized as (7)-(10), respectively.

$$\Delta P=k_{\mathrm{pe}}\Delta E+k_{\mathrm{pd}}\Delta\delta \tag{7}$$

$$\Delta Q=k_{\mathrm{qe}}\Delta E+k_{\mathrm{qd}}\Delta\delta \tag{8}$$

$$\Delta\omega=\Delta\omega^*-k_{\mathrm{p}}\Delta P+k_{\mathrm{p}}\Delta P^* \tag{9}$$

$$\Delta E=\Delta E^*-k_{\mathrm{q}}\Delta Q+k_{\mathrm{q}}\Delta Q^* \tag{10}$$

where $k_{\mathrm{pe}}=\dfrac{3RE}{R^2+X^2}$; $k_{\mathrm{pd}}=\dfrac{3XE^2}{R^2+X^2}$; $k_{\mathrm{qe}}=\dfrac{3XE}{R^2+X^2}$; and $k_{\mathrm{qd}}=\dfrac{-3RE^2}{R^2+X^2}$.

Assuming that ω^*, E^*, P^*, and Q^* are constant, the deviation terms in (9) and (10) can be ignored. To filter out the high-frequency components in the measured power components caused by load unbalance, low-pass filters (LPFs) are typically used in power control loops. These LPFs introduce a multi-time-scale separation between the inner voltage and current loop and the outer power loop, where the latter is more than ten times slower than the former [27], [28]. Hence, the inner loop is often ignored in the modeling process of microgrids [29], [30]. This paper exclusively focuses on the design of an adaptive controller for the power loop. Since the proposed MRAC is an adaptive one, it can compensate for adverse effects of uncertainties including unmodeled dynamics due to ignoring the dynamics of the inner loop. The steady-state values of the frequency and voltage magnitude are achieved through static droop control. Therefore, the local control method of the DG, known as the droop control method (P-ω and Q-E), can be written as:

$$\Delta\omega=-k_{\mathrm{p}}\frac{\omega_{\mathrm{p}}}{s+\omega_{\mathrm{p}}}\Delta P \tag{11}$$

$$\Delta E=-k_{\mathrm{q}}\frac{\omega_{\mathrm{q}}}{s+\omega_{\mathrm{q}}}\Delta Q \tag{12}$$

where ω_{p} and ω_{q} are the cut-off frequencies of the active and reactive power loops, respectively.

By defining the state vector $\boldsymbol{x}(t)=[\Delta\delta(t), \Delta\omega(t), \Delta E(t)]^{\mathrm{T}}$, the state-space representation of the studied system is expressed as:

$$\begin{cases}\dot{\boldsymbol{x}}(t)=\boldsymbol{A}\boldsymbol{x}(t)+\boldsymbol{B}\boldsymbol{u}(t)\\ \boldsymbol{y}(t)=\boldsymbol{C}\boldsymbol{x}(t)\end{cases} \tag{13}$$

where $\boldsymbol{y}(t)$ and $\boldsymbol{u}(t)$ are the system output and the control input, respectively; $\boldsymbol{A}=\begin{bmatrix}0 & 1 & 0\\ -k_{\mathrm{p}}\omega_{\mathrm{p}}k_{\mathrm{pd}} & -\omega_{\mathrm{p}} & -k_{\mathrm{p}}\omega_{\mathrm{p}}k_{\mathrm{pe}}\\ -k_{\mathrm{q}}\omega_{\mathrm{q}}k_{\mathrm{qd}} & 0 & -(\omega_{\mathrm{q}}+k_{\mathrm{q}}\omega_{\mathrm{q}}k_{\mathrm{qe}})\end{bmatrix}$; $\boldsymbol{B}=\begin{bmatrix}0 & k_{\mathrm{p}}\omega_{\mathrm{p}} & 0\\ 0 & 0 & k_{\mathrm{q}}\omega_{\mathrm{q}}\end{bmatrix}^{\mathrm{T}}$; and $\boldsymbol{C}=\begin{bmatrix}0 & 1 & 0\\ 0 & 0 & 1\end{bmatrix}$.

According to (13), the studied system is a two-input two-output (TITO) system; hence, the control inputs can independently regulate two outputs. To investigate this issue, the functional controllability of the system can be used. The transfer function matrix $\boldsymbol{G}(s)$ of (13) is obtained as:

$$\boldsymbol{G}(s)=\boldsymbol{C}(s\boldsymbol{I}-\boldsymbol{A})^{-1}\boldsymbol{B}=\begin{bmatrix}\dfrac{0.003s^2+1.046s}{g(s)} & \dfrac{80.89}{g(s)}\\[2ex] \dfrac{-0.26s}{g(s)} & \dfrac{0.041s^2+1.283s+296.5}{g(s)}\end{bmatrix} \tag{14}$$

where $g(s)=s^3+385.5s^2+1.838\times10^4 s+2.745\times10^6$; and $\boldsymbol{I}$ is the unit matrix.

Definition Consider the transfer function matrix $\boldsymbol{G}(s)$ with m-input l-output. $\boldsymbol{G}(s)$ is functionally controllable provided that the normal rank of $\boldsymbol{G}(s)$ is equal to l [31].

Based on the above definition, the necessary and sufficient condition for the functional controllability of (14) is $|\boldsymbol{G}(s)|\neq 0$. Using the parameters of the studied system [3], as given in Tables I-IV, it can be concluded that the system is functionally controllable since $|\boldsymbol{G}(s)|\neq 0$; therefore, it is possible to achieve two independent objectives. In this paper, the control objective is the VaF regulation of the AC microgrid associated with accurate power sharing.

TABLE I
ELECTRICAL PARAMETERS OF STUDIED SYSTEM

Parameter	Value
DC voltage V_{dc} (V)	690
Switching frequency f_{s} (Hz)	1650
Nominal frequency ω_0 (rad/s)	100π
Nominal voltage amplitude E_0 (V)	$220\sqrt{2}$
Cut-off frequencies ω_{p}, ω_{q} (rad/s)	31.4, 31.4

TABLE II
DG SPECIFICATION OF STUDIED SYSTEM

Parameter	Value	
	DGs 1 and 2	DGs 3 and 4
Resistance of LC filter R_f (Ω)	0.1	0.1
Inductance of LC filter L_f (mH)	1.35	1.35
Capacitance of LC filter C_f (μF)	50	50
Feeder resistance R (Ω)	0.03	0.03
Feeder inductance L (mH)	0.35	0.35
k_p	9.4×10^{-5}	12.5×10^{-5}
k_q	1.3×10^{-3}	1.5×10^{-3}

TABLE III
INNER-LOOP CONTROL PARAMETERS OF STUDIED SYSTEM

Parameter	Value	
	DGs 1 and 2	DGs 3 and 4
Proportional coefficient of voltage controller gain K_{PV}	0.1	0.05
Integral coefficient of voltage controller gain K_{IV}	420	390
Proportional coefficient of current controller gain K_{PC}	15	10.5
Integral coefficient of current controller gain K_{IC}	20000	16000

TABLE IV
LINE PARAMETERS OF STUDIED SYSTEM

Line	Resistance (Ω)	Inductance (μH)
Line 1	0.23	138
Line 2	0.30	600

B. Inertia Control

Droop-based microgrids are generally inertia-less and sensitive to faults. Control methods such as using VSGs and virtual synchronous machines (VSMs) have been suggested to provide inertia support [21], [32]. These methods emulate the transient characteristics of synchronous generators (SGs) by mimicking their basic swing equation. VSGs add virtual inertia to the system, improving the stability and performance of microgrid. As the inertia response is caused by the rotation of heavy mass and is proportional to the rotor speed, VSGs can directly enhance the frequency response. Inadvertently, the usage of LPFs introduces virtual inertia to the DG, similar to the VSG [33]. The swing equation for the VSG control can be expressed as [32], [34]:

$$\Delta\omega = \frac{-1}{J\omega_0 s + D_p}\Delta P \tag{15}$$

where J and D_p are the virtual moment of inertia and the virtual damping factor in the active power loop, respectively. Paying attention to (11), the droop control with an LPF is equivalent to the VSG control. The relations between them can be stated as:

$$\begin{cases} J = \dfrac{1}{\omega_0 k_p \omega_p} \\ D_p = \dfrac{1}{k_p} \end{cases} \tag{16}$$

The droop control (non-inertial) can be considered as a specific case of the inertial one, i.e., $J=0$ or $\omega_p=\infty$. Therefore, it is possible to represent both using a general model. In this paper, the droop control with the LPFs is selected as the representative.

III. DESIGN OF PROPOSED MRAC

The block diagram of the proposed MRAC is presented in Fig. 2. The main components of the proposed MRAC structure include the reference model, controller, and adaptive mechanisms. All control objectives are taken into account in the designed reference model, after which the adaptive mechanisms change the parameters of controller to ensure that the closed-loop control system functions like the reference model. The rest of this section explains the design procedure of the MRAC for the studied DG in detail.

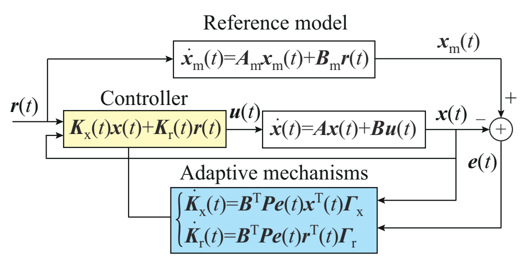

Fig. 2. Block diagram of proposed MRAC.

A. Reference Model Design

Since the state-space representation in (13) is third-order, the following reference model is considered:

$$\dot{\boldsymbol{x}}_m(t)=\begin{bmatrix}-a_{m1} & 0 & 0\\ 0 & -a_{m2} & 0\\ 0 & 0 & -a_{m3}\end{bmatrix}\boldsymbol{x}_m(t)+\begin{bmatrix}0 & 0\\ a_{m2} & 0\\ 0 & a_{m3}\end{bmatrix}\boldsymbol{r}(t)= \boldsymbol{A}_m\boldsymbol{x}_m(t)+\boldsymbol{B}_m\boldsymbol{r}(t) \tag{17}$$

where $\boldsymbol{x}_m(t)$ and $\boldsymbol{r}(t)$ are the state variable vector and the input vector of the reference model, respectively; and a_{m1}, a_{m2}, and a_{m3} are three positive real numbers that have been selected based on time-domain performance criteria such as settling time, rise time, overshoot, and frequency-domain specifications, including phase and gain margins. The reference model (17) has a fully decoupled structure that can provide acceptable performance even in the presence of unknown dynamics. The tracking error $\boldsymbol{e}(t)$ is defined as:

$$\boldsymbol{e}(t)=\boldsymbol{x}_m(t)-\boldsymbol{x}(t) \tag{18}$$

The problem is to design a controller for (13) such that $\boldsymbol{e}(t)$ asymptotically tends to zero, even though $\boldsymbol{A}$ is unknown.

Remark 1 As the design parameters (k_p, k_q, ω_p, and ω_q) are chosen by the designer, $\boldsymbol{B}$ is known. In contrast, $\boldsymbol{A}$ is unknown since it depends on the parameters of feeder line.

B. Controller Structure Selection

A general feedback-feedforward structure is considered for the adaptive controller as:

$$\boldsymbol{u}(t)=\boldsymbol{K}_x(t)\boldsymbol{x}(t)+\boldsymbol{K}_r(t)\boldsymbol{r}(t) \tag{19}$$

where $\boldsymbol{K}_x(t)\in\mathbb{R}^{2\times 3}$ and $\boldsymbol{K}_r(t)\in\mathbb{R}^{2\times 2}$ are the feedback and feedforward gains, respectively.

To track the reference model by the closed-loop system, it is sufficient to select $\boldsymbol{K}_x(t)=\boldsymbol{K}_x^*$ and $\boldsymbol{K}_r(t)=\boldsymbol{K}_r^*$, where $\boldsymbol{K}_x^*$ and $\boldsymbol{K}_r^*$ are ideal gains that are obtained from:

$$\boldsymbol{A}+\boldsymbol{B}\boldsymbol{K}_x^*=\boldsymbol{A}_m \tag{20}$$

$$\boldsymbol{B}\boldsymbol{K}_r^*=\boldsymbol{B}_m \tag{21}$$

The necessary and sufficient condition to have a solution for the pole placement problem (20) is the controllability of the pair $(\boldsymbol{A},\boldsymbol{B})$. By constructing the controllability matrix $\boldsymbol{\Phi}_C=[\boldsymbol{B}\quad \boldsymbol{AB}\quad \boldsymbol{A}^2\boldsymbol{B}]$, it can be observed that it is full-rank, and consequently, this condition holds. Since some parameters of the system are unknown, adaptive mechanisms are needed to estimate the controller parameters $\boldsymbol{K}_x^*$ and $\boldsymbol{K}_r^*$.

C. Adaptive Mechanism Design

The Massachusetts Institute of Technology (MIT) rule and the Lyapunov-based approaches are typical for designing the adaptive mechanism [35]. The MIMO MRAC is designed using the latter technique since the stability of the closed-loop system is guaranteed. To this end, the error dynamics are found using (13), (17), and (19) as:

$$\dot{\boldsymbol{e}}(t)=\dot{\boldsymbol{x}}_m(t)-\dot{\boldsymbol{x}}(t)=\boldsymbol{A}_m\boldsymbol{e}(t)-\boldsymbol{B}\tilde{\boldsymbol{K}}_x(t)\boldsymbol{x}(t)-\boldsymbol{B}\tilde{\boldsymbol{K}}_r(t)\boldsymbol{r}(t) \tag{22}$$

where $\tilde{\boldsymbol{K}}_x(t)=\boldsymbol{K}_x(t)-\boldsymbol{K}_x^*$ and $\tilde{\boldsymbol{K}}_r(t)=\boldsymbol{K}_r(t)-\boldsymbol{K}_r^*$. Now, consider the following Lyapunov candidate function:

$$\begin{aligned}V(\boldsymbol{e}(t),\tilde{\boldsymbol{K}}_x(t),\tilde{\boldsymbol{K}}_r(t))=&\,\boldsymbol{e}^T(t)\boldsymbol{P}\boldsymbol{e}(t)+\mathrm{tr}(\tilde{\boldsymbol{K}}_x(t)\boldsymbol{\Gamma}_x^{-1}\tilde{\boldsymbol{K}}_x^T(t))+\\&\mathrm{tr}(\tilde{\boldsymbol{K}}_r(t)\boldsymbol{\Gamma}_r^{-1}\tilde{\boldsymbol{K}}_r^T(t))\end{aligned} \tag{23}$$

where $\mathrm{tr}(\boldsymbol{X})$ is the trace of the square matrix $\boldsymbol{X}$; $\boldsymbol{\Gamma}_x=\boldsymbol{\Gamma}_x^T\in\mathbb{R}^{3\times 3}$ and $\boldsymbol{\Gamma}_r=\boldsymbol{\Gamma}_r^T\in\mathbb{R}^{2\times 2}$ are two positive-definite adaptation rate matrices for $\boldsymbol{K}_x(t)$ and $\boldsymbol{K}_r(t)$, respectively; and $\boldsymbol{P}=\boldsymbol{P}^T\in\mathbb{R}^{3\times 3}$ is the unique positive-definite solution of the following Lyapunov equation:

$$\boldsymbol{A}_m^T\boldsymbol{P}+\boldsymbol{P}\boldsymbol{A}_m=-\boldsymbol{Q}_m \tag{24}$$

where $\boldsymbol{Q}_m=\boldsymbol{Q}_m^T\in\mathbb{R}^{3\times 3}$ is a positive-definite matrix. Since all the eigenvalues of $\boldsymbol{A}_m$ are strictly positive, (24) has a unique positive-definite solution.

The time derivative of the Lyapunov candidate function is expressed as:

$$\begin{aligned}\dot{V}(\boldsymbol{e}(t),\tilde{\boldsymbol{K}}_x(t),\tilde{\boldsymbol{K}}_r(t))=&-\boldsymbol{e}^T(t)\boldsymbol{Q}_m\boldsymbol{e}(t)+\\&2\mathrm{tr}(\tilde{\boldsymbol{K}}_x(t)(-\boldsymbol{x}(t)\boldsymbol{e}^T(t)\boldsymbol{PB}+\boldsymbol{\Gamma}_x^{-1}\dot{\tilde{\boldsymbol{K}}}_x^T(t)))+\\&2\mathrm{tr}(\tilde{\boldsymbol{K}}_r(t)(-\boldsymbol{r}(t)\boldsymbol{e}^T(t)\boldsymbol{PB}+\boldsymbol{\Gamma}_r^{-1}\dot{\tilde{\boldsymbol{K}}}_r^T(t)))\end{aligned} \tag{25}$$

The following adaptive laws are selected:

$$\dot{\boldsymbol{K}}_x(t)=\boldsymbol{B}^T\boldsymbol{P}\boldsymbol{e}(t)\boldsymbol{x}^T(t)\boldsymbol{\Gamma}_x \tag{26}$$

$$\dot{\boldsymbol{K}}_r(t)=\boldsymbol{B}^T\boldsymbol{P}\boldsymbol{e}(t)\boldsymbol{r}^T(t)\boldsymbol{\Gamma}_r \tag{27}$$

And we have:

$$\begin{aligned}\dot{V}(\boldsymbol{e}(t),\tilde{\boldsymbol{K}}_x(t),\tilde{\boldsymbol{K}}_r(t))=&-\boldsymbol{e}^T(t)\boldsymbol{Q}_m\boldsymbol{e}(t)\le\\&-\lambda_{min}(\boldsymbol{Q}_m)\left\|\boldsymbol{e}(t)\right\|_2^2\le 0\end{aligned} \tag{28}$$

where $\lambda_{min}(\boldsymbol{Q}_m)$ is the smallest eigenvalue of $\boldsymbol{Q}_m$. It can be concluded that $\boldsymbol{e}(t)$, $\tilde{\boldsymbol{K}}_x(t)$, and $\tilde{\boldsymbol{K}}_r(t)$ are bounded due to $\dot{V}(\boldsymbol{e}(t),\tilde{\boldsymbol{K}}_x(t),\tilde{\boldsymbol{K}}_r(t))\le 0$ [35]. To investigate the asymptotic stability of $\boldsymbol{e}(t)$, the following two Lemmas are presented.

Lemma 1 (Barbalat's Lemma) If the differentiable function $f(t)$ has a finite limit as $t\to\infty$ and $\dot{f}(t)$ is uniformly continuous, then $\dot{f}(t)\to 0$ as $t\to\infty$ [25].

Lemma 2 If $\ddot{f}(t)$ is bounded, then $f(t)$ is uniformly continuous [35].

We can compute:

$$\begin{aligned}&\lim_{t\to\infty}V(\boldsymbol{e}(t),\tilde{\boldsymbol{K}}_x(t),\tilde{\boldsymbol{K}}_r(t))=\\&\qquad V(\boldsymbol{e}_0(t),\tilde{\boldsymbol{K}}_{x0}(t),\tilde{\boldsymbol{K}}_{r0}(t))-\lambda_{min}(\boldsymbol{Q}_m)\left\|\boldsymbol{e}(t)\right\|_2^2\end{aligned} \tag{29}$$

where the subscript 0 represent the initial values.

Thus, $V(\boldsymbol{e}(t),\tilde{\boldsymbol{K}}_x(t),\tilde{\boldsymbol{K}}_r(t))$ has a finite limit as $t\to\infty$. Since $\left\|\boldsymbol{e}(t)\right\|_2$ exists, $\boldsymbol{e}(t)\in\mathcal{L}_2\cap\mathcal{L}_\infty$, but $\left\|\dot{\boldsymbol{e}}(t)\right\|\in\mathcal{L}_\infty$, where $\mathcal{L}_2$ is the set of all signals for which the integral of their squared magnitudes over the entire domain is finite; and $\mathcal{L}_\infty$ is the set of bounded signals. $\dot{V}(\boldsymbol{e}(t),\tilde{\boldsymbol{K}}_x(t),\tilde{\boldsymbol{K}}_r(t))$ can be shown to be uniformly continuous by evaluating if its derivative is bounded.

$$\begin{aligned}\ddot{V}(\boldsymbol{e}(t),\tilde{\boldsymbol{K}}_x(t),\tilde{\boldsymbol{K}}_r(t))=&-\dot{\boldsymbol{e}}^T(t)\boldsymbol{Q}_m\boldsymbol{e}(t)-\boldsymbol{e}^T(t)\boldsymbol{Q}_m\dot{\boldsymbol{e}}(t)=\\&-\boldsymbol{e}^T(t)(\boldsymbol{Q}_m\boldsymbol{A}+\boldsymbol{A}^T\boldsymbol{Q}_m)\boldsymbol{e}(t)-2\boldsymbol{e}^T\boldsymbol{Q}_m(\boldsymbol{A}_m\boldsymbol{e}(t)-\\&\boldsymbol{B}\tilde{\boldsymbol{K}}_x(t)\boldsymbol{x}(t)-\boldsymbol{B}\tilde{\boldsymbol{K}}_r(t)\boldsymbol{r}(t))\end{aligned} \tag{30}$$

Since $\boldsymbol{e}(t)$, $\boldsymbol{K}_x(t)$, and $\boldsymbol{K}_r(t)$ are bounded, $\ddot{V}(\boldsymbol{e}(t),\tilde{\boldsymbol{K}}_x(t),\tilde{\boldsymbol{K}}_r(t))$ is bounded. Consequently, $\dot{V}(\boldsymbol{e}(t),\tilde{\boldsymbol{K}}_x(t),\tilde{\boldsymbol{K}}_r(t))$ is uniformly continuous. Using Lemma 1, $\boldsymbol{e}(t)$ is asymptotically stable. Theorem 1 summarizes the stability property of the closed-loop system.

Theorem 1 If $(\boldsymbol{A},\boldsymbol{B})$ is controllable and for any positive-definite $\boldsymbol{Q}_m$, the system (13) under the structure of adaptive controller (19) and the adaptive laws (26) and (27) asymptotically follow the reference model (17).

The main design steps of the proposed MRAC are illustrated in Fig. 3.

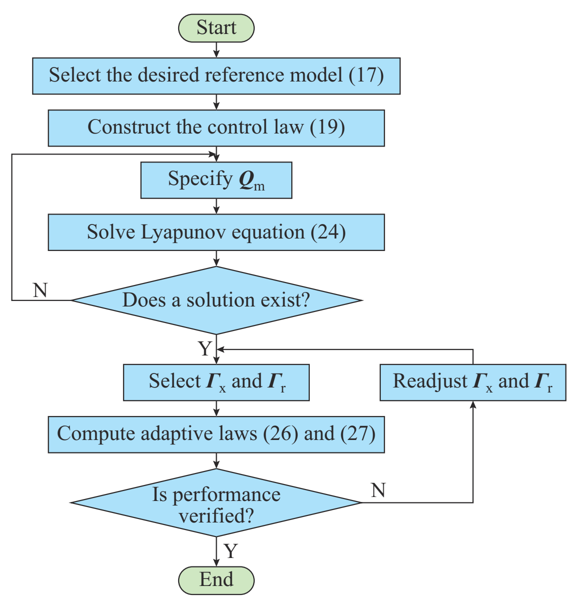

Fig. 3. Main design steps of proposed MRAC.

IV. Simulation Results

The single-line diagram of the studied microgrid is shown in Fig. 4. The proposed MRAC in two scenarios, i.e., droop-based and inertia-based MRAC, is applied to an autonomous AC microgrid consisting of four different DGs that supply three local loads.

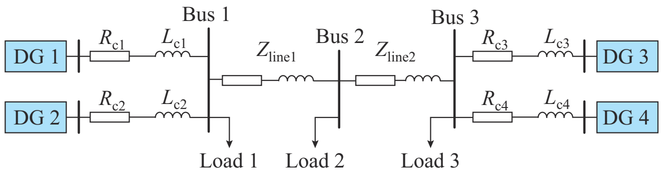

Fig. 4. Single-line diagram of studied microgrid.

Remark 2 The proposed MRAC can be applied to two different types of microgrids: droop-based and inertia-based ones. Droop-based microgrids demonstrate fast dynamic responses due to their inertia-less characteristics. Since inertia-based microgrids prioritize emulating the inertia and kinetic energy of traditional generators to enhance grid stability [34], this type of microgrid is associated with slow dynamics. Paying attention to the different dynamical properties of droop-based and inertia-based microgrids, the key parameters a_{m1}-a_{m3} and $\boldsymbol{Q}_m$ are selected to achieve different performance criteria. For example, for droop-based microgrids, larger values of a_{m1}-a_{m3} are selected in comparison with inertia-based microgrids. Furthermore, $\boldsymbol{Q}_m$ determines the convergence rate of the desired closed-loop system. In the inertia-based microgrids, unlike the droop-based one, this parameter is deliberately set to be a low value to establish a desired closed-loop system characterized by a slow dynamic response.

A. Droop-based MRAC

In this subsection, the ability of the droop-based MRAC to regulate the VaF of microgrid to their desired values is evaluated. To design the MRAC with the desired settling time of approximately 0.1 s and rise time of 0.06 s, without any overshoot, the parameters of (17) are set as $a_{m1}=35$, $a_{m2}=40$, and $a_{m3}=30$. The input vector of reference model is $\boldsymbol{r}(t)=[100\pi,\ 220\sqrt{2}\,]^{\mathrm{T}}$. To attain the control objectives with desired performance, the design parameters are considered as $\boldsymbol{\Gamma}_x=\mathrm{diag}(100, 600, 100)$, $\boldsymbol{\Gamma}_r=\mathrm{diag}(600, 100)$, and $\boldsymbol{Q}_m=\mathrm{diag}(2500, 5000, 2500)$, respectively. It is assumed that at $t=0.3$ s, loads 1 and 3 with values of $S_1=(10+\mathrm{j}2.5)\,\mathrm{kVA}$ and $S_3=(8+\mathrm{j}2.5)\,\mathrm{kVA}$ are applied to the system, respectively. The changes for load 2 are: during $0.3<t<0.6$ s, $S_2=(22+\mathrm{j}17)$ kVA; during $0.6\ \mathrm{s}<t<0.9$ s, $S_2=(12+\mathrm{j}12)\,\mathrm{kVA}$; and during $0.9\ \mathrm{s}<t<1.2$ s, $S_2=(20+\mathrm{j}20)\,\mathrm{kVA}$.

The frequency and voltage of DGs 1-4 with conventional droop controller are shown in Fig. 5(a) and (b), respectively. The conventional droop controller suffers from a steady-state error. Figure 6(a) and (b) shows the frequency and voltage of DGs 1-4 during load changes with the droop-based MRAC, respectively. The droop-based MRAC quickly restores the frequency and voltage of microgrid to 50 Hz and $220\sqrt{2}$ V under the sequential variations of the load, respectively. The active and reactive power of DGs are shown in Fig. 6(c) and (d), respectively, where the accurate power sharing is achieved by the droop-based MRAC without any communication infrastructure. For DG 1, the time evaluation of the controller parameters is shown in Fig. 7. These parameters do not converge to their ideal values in (20) and (21). This fact coincides with the results obtained by Barbalat's Lemma [25], [35]. While the closed-loop system achieves the desired control objectives, the parameters of the droop-based MRAC remain bounded.

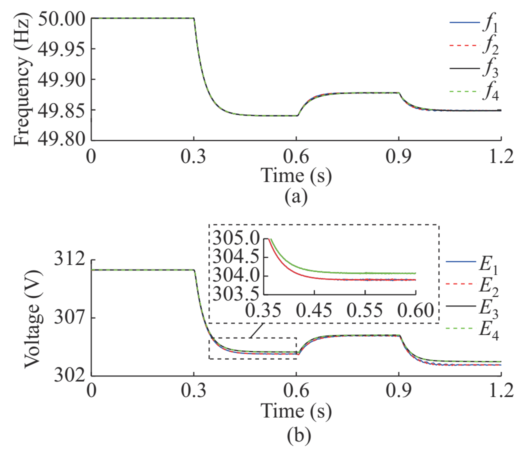

Fig. 5. Frequency and voltage of DGs 1-4 with conventional droop controller. (a) Frequency. (b) Voltage.

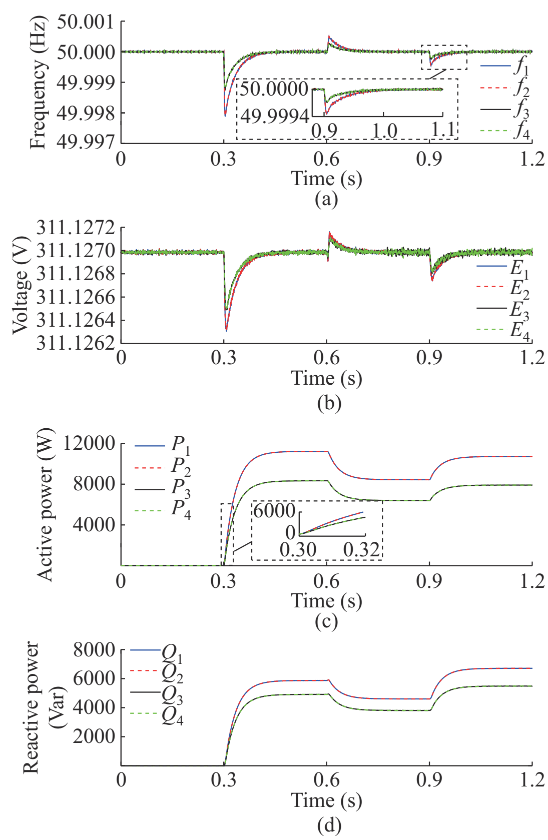

Fig. 6. Simulation results of DGs 1-4 with droop-based MRAC. (a) Frequency. (b) Voltage. (c) Active power. (d) Reactive power.

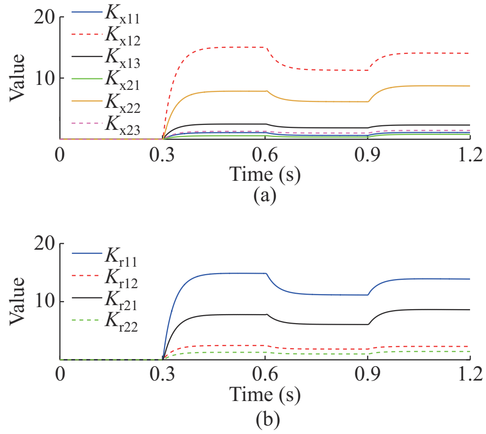

Fig. 7. Controller parameters with droop-based MRAC. (a) Elements of $\boldsymbol{K}_x$. (b) Elements of $\boldsymbol{K}_r$.

To demonstrate the superiority of the droop-based MRAC, a comparison is conducted with an average-based distributed secondary controller. Detailed information about the design procedure of this controller can be found in [7] and [36]. Figure 8 shows the active power of DGs 1-4 with the average-based distributed secondary controller, clearly highlighting the presence of time delays in the zoomed-in plot. Unlike the droop-based MRAC (see Fig. 6(c)), which operates without requiring a communication infrastructure and thus remains unaffected by time delays or communication disturbances, the distributed secondary structure rely on data transmission through communication infrastructure, making them vulnerable to these factors.

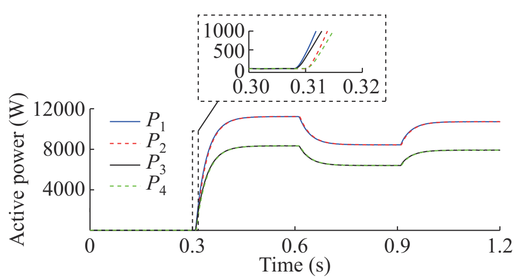

Fig. 8. Active power of DGs 1-4 with average-based distributed secondary controller.

B. Inertia-based MRAC

In this subsection, an inertia-based MRAC is designed to restore the VaF of microgrid. The VSGs are used to virtually inject inertia into the system, thereby enhancing the system stability margin. To achieve the desired closed-loop system, with a settling time of approximately 2.5 s and rise time of 1.5 s, without any overshoot, the reference model parameters in (17) and the design parameters of the controller are selected as $a_{m1}=3$, $a_{m2}=1.5$, $a_{m3}=6$, $\boldsymbol{\Gamma}_x=\text{diag}(9, 15, 9)$, $\boldsymbol{\Gamma}_r=\text{diag}(15, 9)$, and $\boldsymbol{Q}_m=\text{diag}(25, 45, 25)$. At $t=1$ s, loads 1 and 3 with values of $S_1=(10+\text{j}2.5)$ kVA and $S_3=(8+\text{j}2.5)$ kVA are connected to the PCC, respectively. During $1\text{ s}<t<10\text{ s}$ and $10\text{ s}<t<20\text{ s}$, the values of load 2 are $S_2=(12+\text{j}12)$ kVA and $S_2=(22+\text{j}17)$ kVA, respectively. The frequency and voltage of DGs 1-4 with the inertia-based MRAC are shown in Figs. 9(a) and (b), respectively. As can be observed, after some fluctuations around their nominal values, the frequency and voltage are restored to the nominal values with settling time of 2.5 s and 0.65 s, respectively. Figure 9(c) and (d) shows the active and reactive power of DGs 1-4 with the inertia-based MRAC, respectively. The accurate power sharing is achieved in the absence of communication links. In addition, applying the inertia-based MRAC significantly improves the maximum rate-of-change-of-frequency (RoCoF) compared with the droop-based one, which means the system is less sensitive to faults [1], [34].

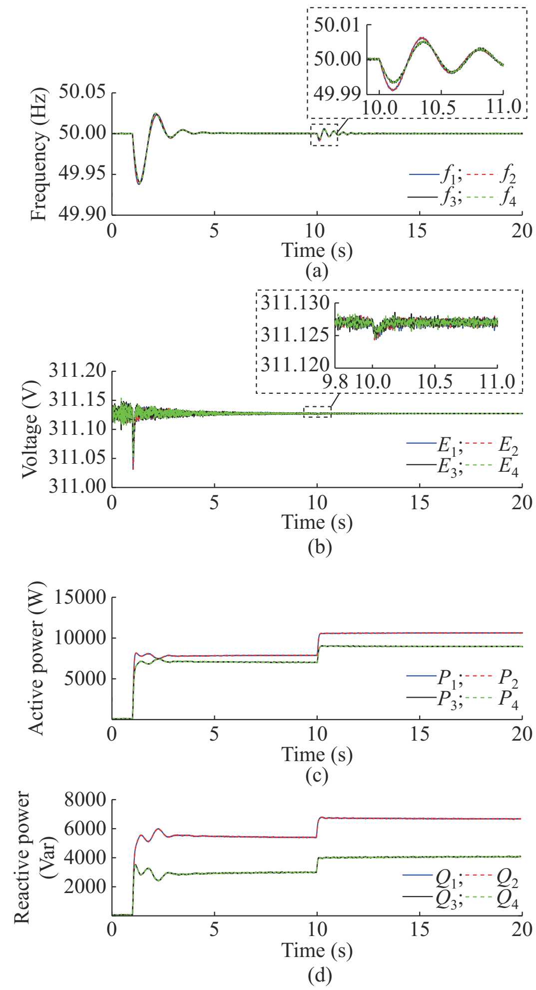

Fig. 9. Simulation results of DGs 1-4 with inertia-based MRAC. (a) Frequency. (b) Voltage. (c) Active power. (d) Reactive power.

C. Impact of Design Parameters

The effects of the design parameters on the frequency of DG 1 are investigated in this subsection. Frequencies with the droop-based and inertia-based MRAC are shown in Figs. 10 and 11, respectively. It is assumed that a load of 5 kW is given to the system at 0.2 s and 1 s. The performance indices under various values of γ and q, with droop-based and inertia-based MRAC, are reported in Tables V and VI, respectively. By choosing larger values of q, it is apparent that both the convergence rate of the closed-loop system and the nadir frequency are significantly improved. In contrast, increasing the adaptation rate γ has a minor effect on enhancing the convergence rate and the nadir frequency. Consequently, the selection of q has a more significant impact on the overall system performance.

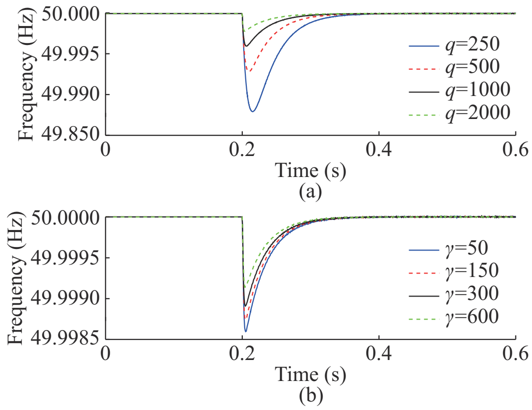

Fig. 10. Frequency of droop-based MRAC. (a) $\boldsymbol{Q}_{\mathrm{m}}(2,2)=q$. (b) $\boldsymbol{\Gamma}_{\mathrm{x}}(2,2)=\gamma$.

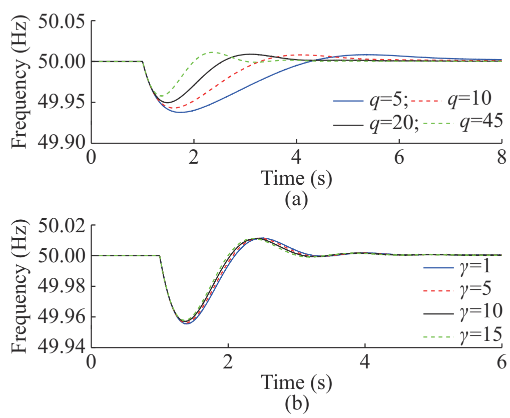

Fig. 11. Frequency of inertia-based MRAC. (a) $\boldsymbol{Q}_{\mathrm{m}}(2,2)=q$. (b) $\boldsymbol{\Gamma}_{\mathrm{x}}(2,2)=\gamma$.

TABLE V
PERFORMANCE INDICES OF DROOP-BASED MRAC UNDER VARIOUS γ AND q VALUES

Parameter	Value	Settling time (s)	Nadir frequency (Hz)
	50	0.12	49.9986
γ	300	0.12	49.9989
	600	0.12	49.9991
	250	0.14	49.9880
q	500	0.11	49.9920
	2000	0.07	49.9980

TABLE VI
PERFORMANCE INDICES OF INERTIA-BASED MRAC UNDER VARIOUS γ AND q VALUES

Parameter	Value	Settling time (s)	Nadir frequency (Hz)
	1	4	49.956
γ	10	4	49.957
	15	4	49.958
	5	7	49.938
q	10	5	49.943
	30	3	49.954

D. Eigenvalues Analysis

The trace of eigenvalues for DG 1 with conventional droop-based controller and proposed droop-based MARC is depicted in Fig. 12, where k_{p} is varied from 9.4×10^{-6} to 9.4×10^{-3}.

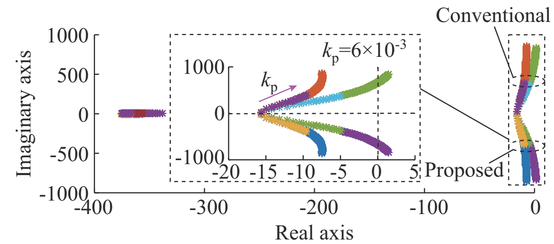

Fig. 12. Trace of eigenvalues with increasing k_{p} from 9.4×10^{-6} to 9.4×10^{-3}.

By increasing k_{p}, the eigenvalues of the open-loop system move towards the right-half plane (RHP), and at $k_{\mathrm{p}}=6\times10^{-3}$, the system becomes unstable. However, with the droop-based MARC, the DG can remain stable even under this condition.

V. CONCLUSION

This paper proposes an MIMO MARC for simultaneous regulation of VaF in autonomous AC microgrids without relying on a communication network. The suggested MARC is designed based on two methods: droop-based and inertia-based methods. The design procedure for the MARC involves three main steps. First, a reference model is constructed using control objectives such as desired settling time, overshoot, and steady-state error. Next, a feedback-feedforward structure is considered for the controller. Finally, two adaptive laws are computed based on Lyapunov's stability theory to achieve the desired closed-loop performance. The effects of the designed parameters on the system performance are investigated in detail, demonstrating that they can be tuned with predictable outcomes. Simulation results confirm the effectiveness of the proposed MIMO MRAC in simultaneously restoring VaF while ensuring accurate power sharing among the DGs.

REFERENCES

[1] H. Bevrani, B. François, and T. Ise, *Microgrid Dynamics and Control*. New York: John Wiley & Sons, 2017.

[2] S. K. Panda and B. Subudhi, "A review on robust and adaptive control schemes for microgrid," *Journal of Modern Power Systems and Clean Energy*, vol. 11, no. 4, pp. 1027-1040, Jun. 2022.

[3] A. Bidram, V. Nasirian, A. Davoudi *et al.*, *Cooperative Synchronization in Distributed Microgrid Control*. New York: Springer, Jan. 2017.

[4] Z. Li, Z. Cheng, J. Si *et al.*, "Distributed event-triggered hierarchical control to improve economic operation of hybrid AC/DC microgrids," *IEEE Transactions on Power Systems*, vol. 37, no. 5, pp. 3653-3668, Dec. 2021.

[5] M. Minetti, A. Rosini, G. B. Denegri *et al.*, "An advanced droop control strategy for reactive power: assessment in islanded microgrids," *IEEE Transactions on Power Systems*, vol. 37, no. 4, pp. 3014-3025, Nov. 2021.

[6] A. Bidram and A. Davoudi, "Hierarchical structure of microgrids control system," *IEEE Transactions on Smart Grid*, vol. 3, no. 4, pp. 1963-1976, May 2012.

[7] Y. Khayat, Q. Shafiee, R. Heydari *et al.*, "On the secondary control ar-

chitectures of AC microgrids: an overview," *IEEE Transactions on Power Electronics*, vol. 35, no. 6, pp. 6482-6500, Nov. 2019.
[8] A. Muhtadi, D. Pandit, N. Nguyen *et al*., "Distributed energy resources based microgrid: review of architecture, control, and reliability," *IEEE Transactions on Industry Applications*, vol. 57, no. 3, pp. 2223-2235, Mar. 2021.
[9] A. Mohammed, S. S. Refaat, S. Bayhan *et al*., "AC microgrid control and management strategies: evaluation and review," *IEEE Power Electronics Magazine*, vol. 6, no. 2, pp. 18-31, Jun. 2019.
[10] M. Ahmed, L. G. Meegahapola, A. Vahidnia *et al*., "Adaptive virtual impedance controller for parallel and radial microgrids with varying *X/R* ratios," *IEEE Transactions on Sustainable Energy*, vol. 13, no. 2, pp. 830-843, Dec. 2021.
[11] H. Morales-Paredes, D. Tardivo, C. D. B. Mellado *et al*., "Enhanced control strategy based on virtual impedance loops to achieve the sharing of imbalance and harmonic in 3-phase 4-wire isolated microgrids," *IEEE Transactions on Power Delivery*, vol. 37, no. 4, pp. 3412-3415, Feb. 2022.
[12] A. Vijay, N. Parth, S. Doolla *et al*., "An adaptive virtual impedance control for improving power sharing among inverters in islanded AC microgrids," *IEEE Transactions on Smart Grid*, vol. 12, no. 4, pp. 2991-3003, Feb. 2021.
[13] Z. Li, K. W. Chan, J. Hu *et al*., "Adaptive droop control using adaptive virtual impedance for microgrids with variable PV outputs and load demands," *IEEE Transactions on Industrial Electronics*, vol. 68, no. 10, pp. 9630-9640, Sept. 2020.
[14] A. K. Sahoo, K. Mahmud, M. Crittenden *et al*., "Communication-less primary and secondary control in inverter-interfaced AC microgrid: an overview," *IEEE Journal of Emerging and Selected Topics in Power Electronics*, vol. 9, no. 5, pp. 5164-5182, Feb. 2020.
[15] R. Heydari, T. Dragičević, and F. Blaabjerg, "High-bandwidth secondary voltage and frequency control of VSC-based AC microgrid," *IEEE Transactions on Power Electronics*, vol. 34, no. 11, pp. 11320-11331, Feb. 2019.
[16] K. Ahmed, M. Seyedmahmoudian, S. Mekhilef *et al*., "A review on primary and secondary controls of inverter-interfaced microgrid," *Journal of Modern Power Systems and Clean Energy*, vol. 9, no. 5, pp. 969-985, Dec. 2020.
[17] W. Liu, J. Shen, S. Zhang *et al*., "Distributed secondary control strategy based on *Q*-learning and pinning control for droop-controlled microgrids," *Journal of Modern Power Systems and Clean Energy*, vol. 10, no. 5, pp. 1314-1325, Aug. 2022.
[18] L. Yan, M. Sheikholeslami, W. Gong *et al*., "Architecture, control, and implementation of networked microgrids for future distribution systems," *Journal of Modern Power Systems and Clean Energy*, vol. 10, no. 2, pp. 286-299, Mar. 2022.
[19] M. Hua, H. Hu, Y. Xing *et al*., "Multilayer control for inverters in parallel operation without intercommunications," *IEEE Transactions on Power Electronics*, vol. 27, no. 8, pp. 3651-3663, Feb. 2012.
[20] H. Xin, L. Zhang, Z. Wang *et al*., "Control of island AC microgrids using a fully distributed approach," *IEEE Transactions on Smart Grid*, vol. 6, no. 2, pp. 943-945, Dec. 2014.
[21] K. Jiang, H. Su, H. Lin *et al*., "A practical secondary frequency control strategy for virtual synchronous generator," *IEEE Transactions on Smart Grid*, vol. 11, no. 3, pp. 2734-2736, Feb. 2020.
[22] Y. Khayat, M. Naderi, Q. Shafiee *et al*., "Decentralized optimal frequency control in autonomous microgrids," *IEEE Transactions on Power Systems*, vol. 34, no. 3, pp. 2345-2353, Dec. 2018.
[23] B. Liu, T. Wu, Z. Liu *et al*., "A small-AC-signal injection-based decentralized secondary frequency control for droop-controlled islanded microgrids," *IEEE Transactions on Power Electronics*, vol. 35, no. 11, pp. 11634-11651, Mar. 2020.
[24] J. M. Rey, P. Martí, M. Velasco *et al*., "Secondary switched control with no communications for islanded microgrids," *IEEE Transactions on Industrial Electronics*, vol. 64, no. 11, pp. 8534- 8545, May. 2017.
[25] N. T. Nguyen, *Model-reference Adaptive Control*. New York: Springer, 2018.
[26] R. Wang, Q. Sun, D. Ma *et al*., "The small-signal stability analysis of the droop-controlled converter in electromagnetic timescale," *IEEE Transactions on Sustainable Energy*, vol. 10, no. 3, pp. 1459-1469, Jan. 2019.
[27] R. K. Sharma, S. Mishra, and D. Pullaguram, "A robust H_∞ multivariable stabilizer design for droop based autonomous AC microgrid," *IEEE Transactions on Power Systems*, vol. 35, no. 6, pp. 4369-4382, Jun. 2020.
[28] H. Yuan, X. Yuan, and J. Hu, "Modeling of grid-connected VSCs for power system small-signal stability analysis in DC-link voltage control timescale," *IEEE Transactions on Power Systems*, vol. 32, no. 5, pp. 3981-3991, Jun. 2017.
[29] S. D. J. M. Machado, S. A. O. da Silva, J. R. B. de A. Monteiro *et al*., "Network modeling influence on small-signal reduced-order models of inverter-based AC microgrids considering virtual impedance," *IEEE Transactions on Smart Grid*, vol. 12, no. 1, pp. 79-92, Jul. 2020.
[30] P. Vorobev, P.-H. Huang, M. A. Hosani *et al*., "High-fidelity model order reduction for microgrids stability assessment," *IEEE Transactions on Power Systems*, vol. 33, no. 1, pp. 874-887, May 2017.
[31] C. Commault, J. van der Woude, and P. Frasca, "Functional target controllability of networks: structural properties and efficient algorithms," *IEEE Transactions on Network Science and Engineering*, vol. 7, no. 3, pp. 1521-1530, Aug. 2019.
[32] A. Rafiee, Y. Batmani, F. Ahmadi *et al*., "Robust load-frequency control in islanded microgrids: virtual synchronous generator concept and quantitative feedback theory," *IEEE Transactions on Power Systems*, vol. 36, no. 6, pp. 5408-5416, May 2021.
[33] D. Pan, X. Wang, F. Liu *et al*., "Transient stability of voltage-source converters with grid-forming control: a design-oriented study," *IEEE Journal of Emerging and Selected Topics in Power Electronics*, vol. 8, no. 2, pp. 1019-1033, Oct. 2019.
[34] J. Liu, Y. Miura, H. Bevrani *et al*., "Enhanced virtual synchronous generator control for parallel inverters in microgrids," *IEEE Transactions on Smart Grid*, vol. 8, no. 5, pp. 2268-2277, Feb. 2016.
[35] K. J. Åström and B. Wittenmark, *Adaptive Control*. Chigaco: *Courier Corporation*, Apr. 2013.
[36] Q. Shafiee, J. M. Guerrero, and J. C. Vasquez, "Distributed secondary control for islanded microgrids – a novel approach," *IEEE Transactions on Power Electronics*, vol. 29, no. 2, pp. 1018-1031, Apr. 2013.

Farahnaz Ahmadi received the Ph.D. degree in electrical engineering from the University of Kurdistan, Sanandaj, Iran, in 2023, with honors. Her research interests include robust, adaptive, and nonlinear control with applications in microgrids, power electronics converters, and power systems.

Yazdan Batmani received the B.Sc. degree in biomedical engineering from the University of Isfahan, Isfahan, Iran, in 2006, and the M.Sc. and Ph.D. degrees in control engineering from the K.N. Toosi University of Technology, Tehran, Iran, in 2009 and 2014, respectively. From 2015 to 2019, he was an Assistant Professor with the Department of Electrical Engineering, University of Kurdistan, Sanandaj, Iran, where he is currently an Associate Professor. His current research interests include nonlinear control systems, networked control systems, safety critical control systems, applications of control theory in biomedical engineering, robotics, microgrids, and power systems.

Hassan Bevrani received the Ph. D. degree in electrical engineering from Osaka University, Osaka, Japan, in 2004. He is currently a Professor and the Program Leader of Smart/Micro Grids Research Center with the University of Kurdistan, Sanandaj, Iran. His current research interests include smart grid operation and control, power systems stability and optimization, microgrid dynamics and control, and intelligent/robust control applications in power electric industry.